Optogenetic control of a GEF of RhoA uncovers a signaling switch from retraction to protrusion

Jean De Seze[1], Maud Bongaerts[1], Benoit Boulevard[1], Mathieu Coppey[1]

[1] Laboratoire Physico Chimie Curie, Institut Curie, PSL Research University, Sorbonne Université, CNRS UMR168,

75005 Paris, France

Abstract

The ability of a single signaling protein to induce distinct cellular processes is a well-known feature of cell signaling networks. This assumes that proteins can switch their function depending on the cellular context. However, causally proving and understanding such a switch is an arduous task because of the multiple feedbacks and crosstalks. Here, using an optogenetic tool to control membrane localization of RhoA nucleotide exchange factors (GEFs), we show that a single protein can trigger either protrusion or retraction when recruited to the plasma membrane, polarizing the cell in two opposite directions. We found that the switch from retraction to protrusion is due to the increase of the basal concentration of the GEF prior to activation. The unexpected protruding behavior arises from the simultaneous activation of Cdc42 and inhibition of RhoA by the PH domain of the GEF at high concentrations. We propose a minimal model and use its predictions to control the two phenotypes within selected cells by adjusting the frequency of light pulses. Our work exemplifies a unique case of control of antagonist phenotypes by a single protein that switches its function based on its concentration or dynamics of activity. It raises numerous open questions about the link between signaling protein and function, particularly in contexts where proteins are highly overexpressed, as often observed in cancer.

Introduction

In cell signaling networks, some key signaling proteins can trigger distinct cellular responses. The specificity of the signal transduced by such proteins is not only encoded in their biochemical state, but also in their dynamics[1]. Most classical examples, such as ERK[2], p53[4] or NF-κB[6], rely on transcriptional regulation, where cell fate is determined over multiple hours. Yet it remains to be addressed whether this multiplexing ability is also a common feature at the minute timescale, where only protein-protein interactions are involved.

To tackle this question, we investigated two fast cell morphological changes occurring simultaneously during cell migration, namely protrusion and retraction[3]. Usually, they are thought to be spatially and temporally controlled by the segregation of protein activities or components within the cell space. Key controllers of these two processes are the members of the Rho family of small GTPases, in particular the three best known RhoA, Rac1, and Cdc42 [5]. These small proteins are turned on in their active GTP form by a large variety of guanine exchange factors (GEFs) and turned off in the GDP form by GTPase activating proteins (GAPs) [7]. Early experiments expressing these GTPases in their active forms [8] led to the canonical picture in which Rac1 and Cdc42 promotes protrusion, with the presence of ruffles and filopodia, while RhoA promotes retraction, as testified by cell rounding and actomyosin contractility.

Yet, a large body of works on the regulation of GTPases has revealed a much more complex picture with numerous crosstalks and feedbacks allowing the fine spatiotemporal patterning of GTPase activities[9]; hereby questioning the legitimacy of the simple canonical picture. This is especially true for RhoA, since it has been proposed to be responsible for both protrusion or retraction depending on the

cellular context [10–12]. It thus remains to be addressed whether the induction of protrusions and retractions are simply set by the independent and segregated activities of GTPases or set by a more complicated signal integration.

In recent years, optogenetics has emerged as a very powerful tool to go beyond correlations and to demonstrate causality in this question. Up to now, the optogenetic approaches that have been developed to control GTPases in space and time tended to confirm the canonical picture. We and others have shown that for Rac1 and Cdc42, the recruitment at the plasma membrane of minimal GEF activating domains causally induces cell protrusions [13] and migration led by the front [14], despite a complex cross-activation between the two signaling proteins. Along the same line, optogenetic approaches to control RhoA, reviewed in [15] and [16], have all shown a causal induction of cell retraction.

Here, contrarily to previous optogenetic approaches, we report that the optogenetic recruitment at the plasma membrane of GEFs of RhoA triggers either protrusion or retraction in the same cell type, polarizing the cell in opposite directions. One GEF of RhoA, PDZ-RhoGEF (PRG), also known as ARHGEF11, was most efficient in eliciting both phenotypes. We show that the outcome of the optogenetic perturbation can be predicted by the basal GEF concentration prior to activation. At high concentration, we demonstrate that Cdc42 is activated together with an inhibition of RhoA by the GEF leading to a cell protrusion. Thanks to the prediction of a minimal mathematical model, we can induce either protrusion or retraction in the same cell by modulating the frequency of light pulses. Our ability to control both phenotypes with a single protein on timescales of second provides a clear and causal demonstration of the multiplexing capacity of signaling circuits solely based on protein-protein interactions.

Local optogenetic recruitment to the plasma membrane of a DH-PH domain of RhoA GEF can lead to both protrusion and retraction in single cells

To control the activity of RhoA in migrating cells, we developed optogenetic tools based on the iLID-SspB light-gated dimerization system to recruit activating domains of GEFs specific to RhoA (**Figure 1A**). Using a strategy already applied to other GTPases [17] and to RhoA itself [18], we anchored the iLID part of the dimer to the membrane thanks to a CAAX motif together with the fluorescent protein mVenus, and expressed in the cytosol the DH-PH domains of different GEFs of RhoA fused to the SspB protein (**Figure 1B**). We cloned the iLID-SspB dimers into a plasmid separated by a P2A motif so that they were expressed at a one-to-one ratio. We selected three of the best-known GEFs of RhoA: LARG (ARHGEF12), GEF-H1 (ARHGEF2), and PDZ-RhoGEF (ARHGEF11). The LARG DH domain was already used with the iLid system [19], the GEF-H1 DH domain had been recruited by optochemical methods [20], and PRG was used with the CRY2-CIBN system [21]. We chose to add the PH domains of GEFs in our constructs since it participates to an auto-amplification process [22] and appears to be sometimes required for GEF specificity [23]. All strategies developed so far have been shown to trigger cell contractility, either in single cells or in monolayers.

We then transiently transfected RPE1 cells with our optogenetic systems (henceforth called optoPRG, optoLARG, and optoGEF-H1) and examined the effects of pulsatile local activation done thanks to a digital micromirror light source (see **material and methods**). In all cases, we saw a clear recruitment of the cytosolic part to the plasma membrane, between 3 and 10 folds, depending on the transfection intensity and the amount of light sent to the sample.

To our surprise, recruitment of DH-PH domains of the three GEFs of RhoA to the membrane with the same experimental procedure resulted in very different phenotypes (**Figure 1C,D** and **Supp Movie 1-2**). Whereas the optoLARG elicited only the expected retractile phenotype typical of RhoA pathway (**Supp Movie 2**), optoGEF-H1 and optoPRG exhibited less predictable behavior (**Figure 1D**). The retractile phenotype was observed in many cells, but a large proportion of cells showed a seemingly opposite response, namely a clear protruding phenotype with filopodia and ruffles (**Figure 1C**). For optoGEF-H1, most of the cells were very round after transfection and showed no response at all after optogenetic recruitment of the DH-PH domain to the membrane. Only few cells (~40%) showed distinct morphological changes after activation, most of them retracted, but some also showed a clear protruding phenotype (**Supp Movie 2**). For optoPRG, most cells showed a distinct phenotypic response upon blue light exposure (**Figure 1D**). Almost 35% of the cells exhibited a clear retracting phenotype leading to the formation of blebs or protrusions at the other side of the cell (**Supp Movie 1**), while 40% exhibited a markedly protruding phenotype (**Supp Movie 1**), reminiscent of the effect of an optoGEF for Cdc42 or Rac1 [13] and often leading to retraction of the other non-activated pole of the cell. A small fraction of cells (~10%) showed no clear response, and the remaining cells (~25%) showed a mixed phenotype: while we could see ruffles or filopodia forming at the site of activation, the cell did not move and appeared to contract at the same time, leading to blebs at the other pole of the cell (**Supp Figure 1**).

To classify the different phenotypes in an unbiased manner, we computed the evolution of the membrane area inside the activation square during the activation with (**Figure 1E**) or without light (**Figure 1F**). We could see the clear impact of the recruitment of the optoPRG, that either triggers a diminution of membrane area -a retraction- or an increase in membrane area -a protrusion-, while control cells show a much smaller membrane movement over the time course of the experiment.

To ensure that the cell response was not due to an already set polarity, we repeated the activation at the other pole of the cell one hour after the first round of activation, when cells had recovered from the first activation and were back to a resting state. Almost all cells retained the same phenotype: they protruded when they were already protruding and retracted when they were already retracting (**Figure 1G-I**). Only few cells showed a mixed phenotype in the first or second round, whereas their phenotype was clear for the other round (**Figure 1H**). Thus, we concluded that for one type of optogenetic activation (one frequency and one light intensity), the phenotype triggered by the recruitment of the optoPRG to the membrane was determined by the state of the cell and not by the cell section in which the optogenetic activation was performed.

To further verify that these opposite phenotypes were not cell line specific, we performed the experiment in Hela cells. The two phenotypes could be observed after transient transfection with optoPRG and activation with the same protocol (**Supp Figure 1**), showing that these two opposites phenotypes are not restricted to RPE1 cells only. Thus, the DH-PH domain of PRG can induce both retraction and protrusion upon its recruitment in single cells. These opposite phenotypes occur in the same cell line, in the same biomechanical environment, and with the same dynamics of recruitment to the membrane. This dual behavior is not cell-specific or exclusive to this GEF of RhoA, as it has also been observed with GEF-H1, although with much less efficiency. For the rest of our study, we focused on optoPRG that elicits the strongest and most reproducible opposing phenotypes.

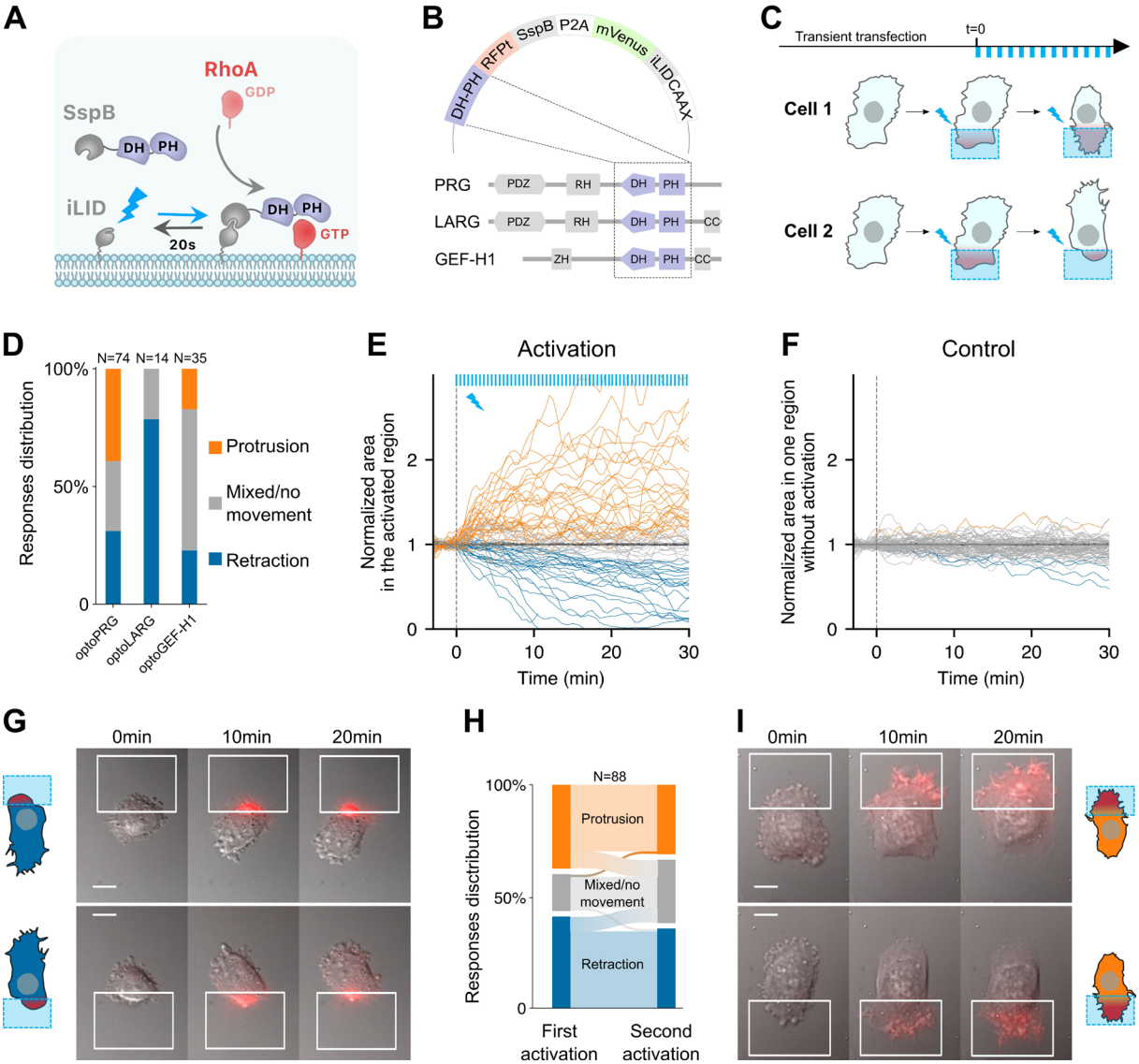

Figure 1: optogenetic activation of RhoA leads to protrusion or retraction. (**A**) Scheme of the optogenetic tool. Optogenetic dimer (in gray) dimerizes upon blue light activation (blue arrow), and dissociates in the dark with an off rate of 20s (black arrow). DH-PH domain is fused to the SspB moiety (purple), which recruitment to the plasma membrane through iLID triggers RhoA activation, from GDP (light red) to GTP (dark red) state. (**B**) The three opto plasmids, with DH-PH domains (purple) shown in their wildtype position in the different RhoA GEFs used here. (**C**) Experimental timeline. Transient transfection is done at least 30 hours before local activation (blue squares). Activation is done by pulses (blue bars, top) at different frequencies, intensities and durations. Cells are observed for 30 to 60 minutes. (**D**) Responses distributions for each optogenetic tool. (**E**,**F**) Area over time of the cell in the activated region (**E**) or without activation (**F**), normalized by the mean initial area. t=0 is the starting point of the activation, each blue bar on top representing one light impulse. Orange: protruding cells, blue: retracting cells, gray: nonmoving cells or mixed phenotype (labeled by hand). (**G**,**I**) representative cells doing retraction (on the left) and protrusion (on the right) upon optogenetic activations on two different side of the cell. Scale bar: 10 µm. White squares: area of activation. Red color: RFPt channel (optogenetic tool). (**H**) Sankey diagram representing the proportion of cells doing a protrusion (orange), retraction (blue) or a mixed phenotype (gray) at one side (first activation) or the other side (second activation).

Cell phenotype upon optogenetic activation depends on the cytosolic concentration of exogenous optoPRG

We next wonder what could differ in the activated cells that lead to the two opposite phenotypes. As all the experiments above were done by transiently transfecting cells, the cell-to-cell variability of

expression led to a wide range of cytosolic concentrations of optoPRG that we can estimate by measuring the mean fluorescence intensity. Looking at the area in the activated region after 5 minutes against the cytosolic concentration of optoPRG leads to very clear result (**Figure 2A**). Below a specific concentration threshold (~40 a.u.), almost all the activated cells (~95%) retract their membrane within the activation area, while above this threshold, ~85% of the cells extend their membrane (see **Figure 2B** for selected examples). This result clearly demonstrates that the phenotype triggered by the activation of optoPRG can be predicted by its concentration within the cell before activation.

This leads to two hypotheses. Either the cell is responding to differences in the absolute amount of optoPRG recruited at the membrane, or the cell is in a different state before optogenetic activation that leads to opposite responses to optoPRG activation. To exclude one of these hypotheses, we first looked at the absolute recruitment at the membrane (**Figure 2C**). Even if the absolute recruitment depends on the initial concentration, we saw a lot of retracting cells reaching very high absolute optoPRG recruitment levels, which tends to exclude the first hypothesis. To further demonstrate it, we overexpressed in a different fluorescent channel a non-recruitable DH-PH domain of PRG, together with the optoPRG, in order to decouple global and recruited PRG concentration. We saw that overexpressing PRG DH-PH strongly increased the number of protruding phenotypes in low expressing cells (from 0% to 45%, **Figure 2D**). Moreover, it was clear that the phenotype switch also correlates with the initial concentration of overexpressed PRG DH-PH domain, highly expressing cells being more prone to protrude (orange dots on the left, **Figure 2D**).

Given that the phenotype switch appeared to be controlled by the amount of over-expressed optoPRG, we hypothesized that the corresponding leakiness of activity could influence the cell state prior to any activation. We first measured the average cell area before activation in the two phenotypes, and saw a strong and significant difference, highly expressing cells being 1.5 times bigger than low expressing cells (**Figure 2E**). We then looked at membrane ruffles without any optogenetic activation, by calculating the mean absolute speed of membrane displacement in one region. We also observed a significant difference, protruding cells having more and stronger membrane displacements before being activated (**Supp Figure 2**).

This series of experiments led us to the conclusion that the main determining factor of the phenotype is the cytosolic concentration of the DH-PH domain of PRG before the optogenetic activation. This initial concentration changes the cell state, in a way that the recruitment of the DH-PH domain of PRG triggers opposite cellular responses.

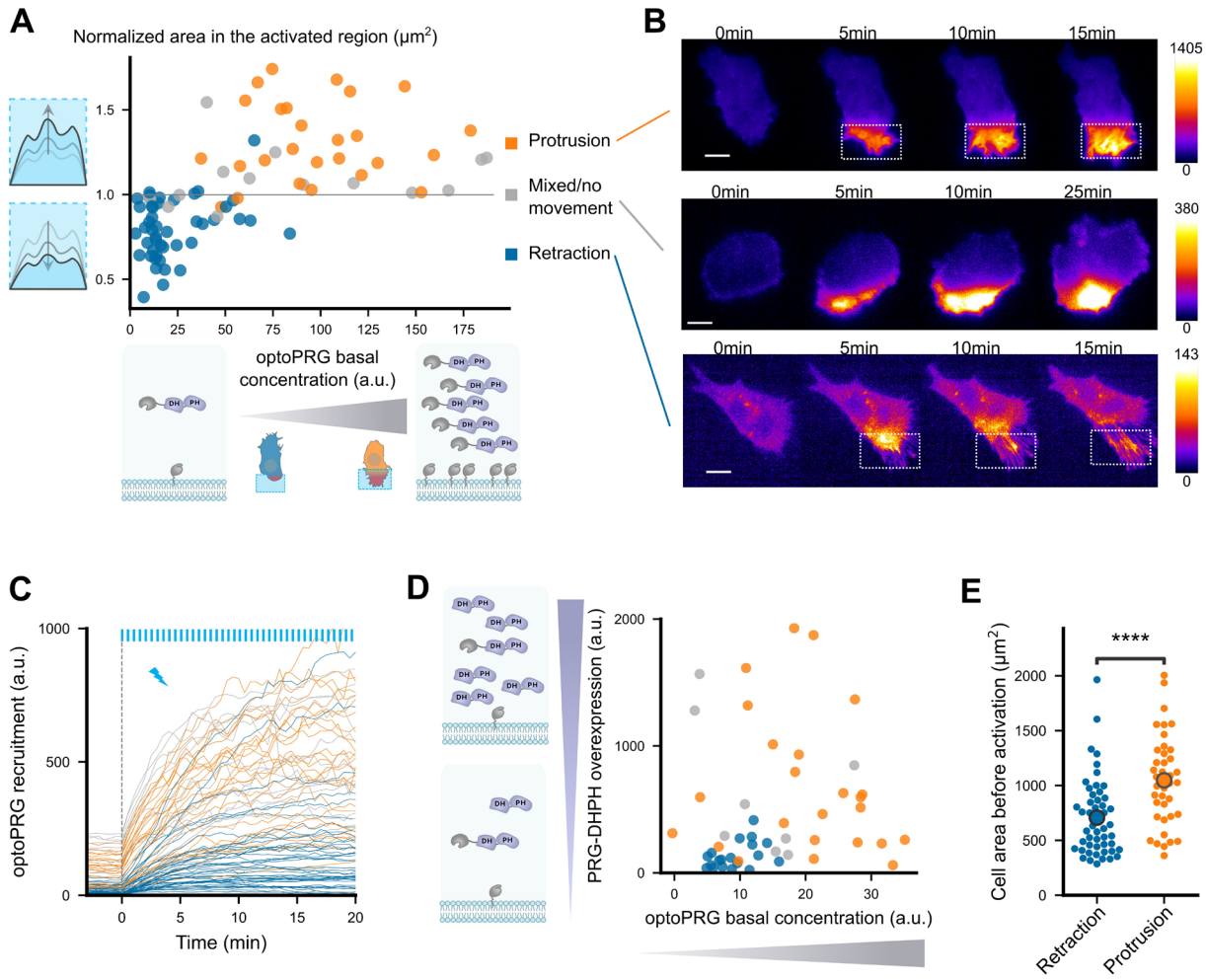

Figure 2: cell phenotype depends on the initial optoPRG concentration. (A) Phenotype dependence on initial cytosolic optoPRG concentration. The normalized area in the activated region after 5 minutes is plotted against the mean fluorescence intensity for each cell, which color is labeled by hand depending on the observed phenotype. Schemes on the bottom represent high and low levels of expression (P2A plasmids implies approximately a one-to-one ratio of iLID against SspB). **(B)** Three representative time lapse images of transiently transfected cells, one retracting (top), one showing a mixed phenotype (middle), and one protruding (bottom). Intensities are very different, as seen by the dynamic range of the colormaps presented on the right. (**C**) Absolute fluorescence intensity of recruited optoPRG, before (t<0) and after (t>0) activation. Blue bars: activation pulses. (**D**) Phenotype depending on both optoPRG concentration and PRG DH-PH overexpression, measured both by fluorescence intensity (a.u.). Increasing recruitable and non-recruitable DH-PH domain of PRG both lead to protruding phenotypes. Phenotypes are manually labelled. (**E**) Cell area before activation for retracting (blue) and protruding (orange) cells. (Mann–Whitney U test. **** <0.0001)

Two distinct signaling pathways are triggered from the first activation timepoint

Very surprised by this ability of one protein to trigger opposite phenotypes, we sought to further characterize these responses by monitoring the activity of key proteins involved in the RhoA pathway. To this end, we initially investigated whether the variation in actin and myosin levels following optogenetic activation corresponded to the stereotypical dynamics of protrusions and retractions described in a previous study by Martin *et al.* [24]. We thus monitored Lifeact-iRFP and MRLC-iRFP (Myosin regulatory light chain) proteins during the optogenetic experiments. In the retraction phenotype, the first recruitment of optoPRG to the membrane was followed by an immediate polymerization of actin in the area of activation, as we quantified over multiple experiments (**Figure**

3A-C). Myosin recruitment appeared to follow the polymerization of actin, leading to the retraction of the membrane in the minutes following the activation (**Figure 3D-F**). In contrast, when cells were protruding, we observed a decrease in MRLC and Lifeact intensities following the first activation of our tool by light (**Figure 3A-F**), as it was previously shown for protrusions triggered by PDGF [24]. This first decrease is probably due to the depolymerization of stress fibers at the area of activation. It is followed by an increase in actin polymerization, most probably responsible for the net displacement of the membrane, while myosin stays lower than the initial state. These differences in actin and myosin dynamics for the two phenotypes are visible at 30 seconds, one frame after the first pulse of light (**Figure 3C,F**), even if the cell phenotype cannot be distinguished by eye before one or two minutes. This shows that the pathways triggered by optoPRG recruitment differs from the first tens of seconds after light activation. We thus turned to RhoA itself, which is supposed to be upstream of actin and myosin, and just downstream of PRG. As our optogenetic tool prevented us from using FRET biosensors because of spectral overlap, we turned to a relocation biosensor that binds RhoA in its GTP form [25]. This highly sensitive biosensor is based on the multimeric TdTomato, whose spectrum overlap with the RFPt fluorescent protein used for quantifying optoPRG recruitment. We thus designed a new optoPRG with iRFP, which could trigger both phenotypes but was harder to transiently express, giving rise to a majority of retracting phenotype. Looking at the RhoA biosensor, we saw very different responses for both phenotypes (**Figure 3G-I**). While retracting cells led to strong and immediate activation of RhoA, protruding cells showed a much smaller and delayed response. After the first minute of optogenetics activation, no significant change was seen in protruding cells (**Figure 3I**). Thus, either an unknown factor is sequestering RhoA-GDP, or optoPRG preferentially binds to another partner, both hypotheses being non-mutually exclusive.

Altogether, these data demonstrate that cells exhibit very different responses to optoPRG activation, regarding both actin polymerization and myosin activity, and even RhoA activity itself. They show that different pathways are immediately engaged, already at the level of Rho-GTPases, few tens of seconds after the first optogenetic activation.

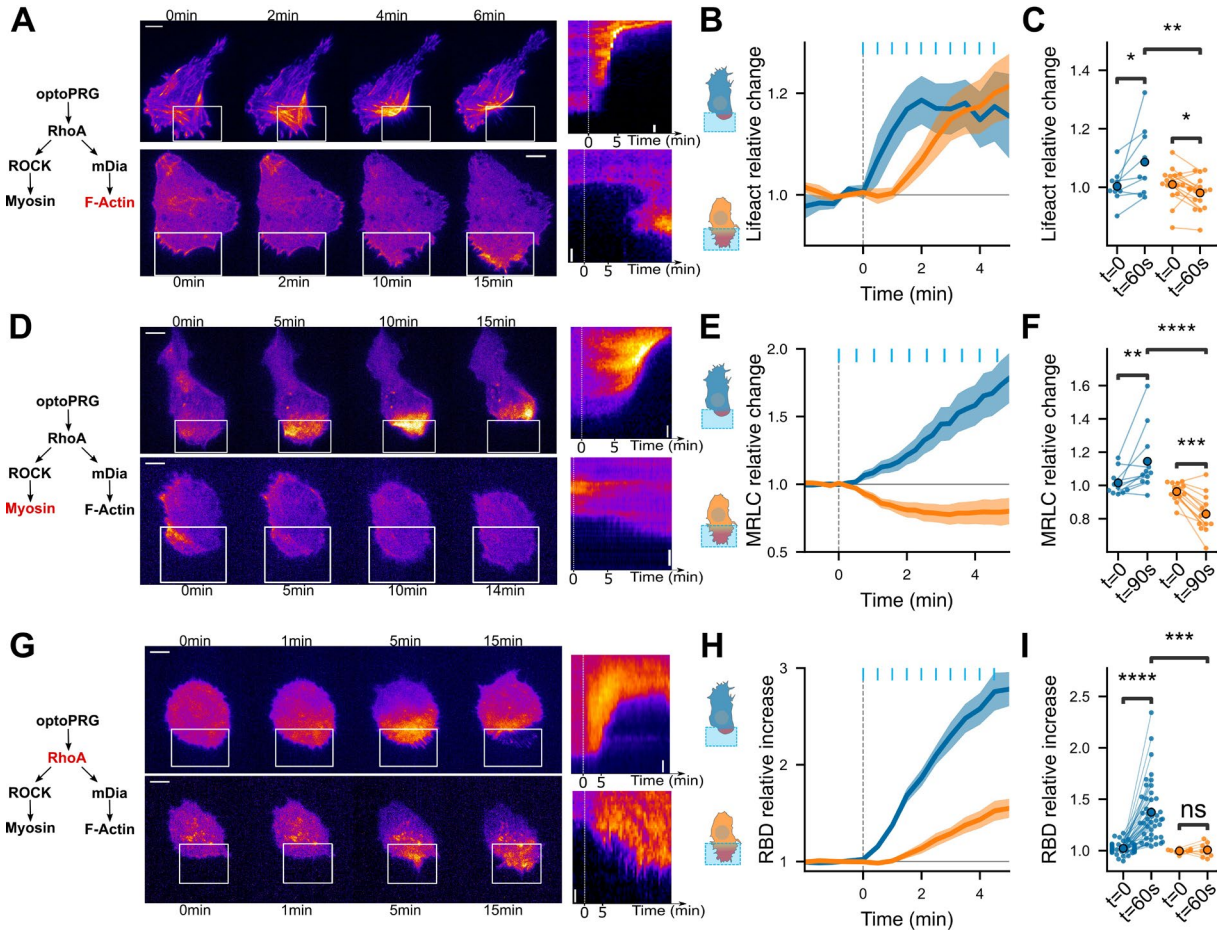

Figure 3: downstream effectors show that cell phenotype is set immediately. Distinct pathways are triggered from the first timepoint. (**A**,**D**,**G**) Representative timelapse images and kymographs of retracting (top) and protruding (bottom) cells labeled with Lifeact-iRFP (**A**), MRLC-iRFP(**D**), and RBD-2xTdTomato biosensor (**G**), activated with optoPRG starting at t=0min. White rectangles are areas of optogenetic activation. Scale bars are 10 µm. (**B**,**E**,**H**) Corresponding mean normalized intensities are plotted against time (mean +/- s.e.m.), blue for retracting cells and orange for protruding one. (**C**,**F**,**I**) Corresponding pairwise comparison for each cell of the signal inside the region of activation between the initial time and 60s (Lifeact-iRFP and RhoA biosensor) or 90s (MRCL-iRFP). Data are grouped by phenotype. *P<0.05 **P<0.01, ***P<0.001, **** P<0.0001 (Wilcoxon test to compare t=0 and t>0, independent t-test otherwise)

PH domain of PRG can inhibit RhoA and is necessary for the protruding phenotype

As the phenotype triggered by optoPRG, revealed on a minute timescale, seems to be set by the reactions of the intracellular biochemical network after few tens of seconds, we turned to an analysis of RhoA activity at smaller timescale. Our first surprise came while looking at the response of the RhoA biosensor to pulses of optoPRG activation. We show in **Figure 4A** three representative examples of such responses. While at low optoPRG concentration (cell 1), RhoA activity follows the pulses of optoPRG with some delay, at higher concentrations (cell 2 and cell 3), RhoA activity shows a very different behavior: it first decays, and then rise. It seems that, adding to the well-known activation of RhoA, PRG DH-PH can also negatively regulate RhoA activity.

Knowing that the PH domain of PRG triggers a positive feedback loop thanks to its binding to active RhoA [22], we hypothesized that this binding could sequester active RhoA at high optoPRG levels, thus being responsible for its inhibition. To test our hypothesis, we designed a new optogenetic tool to recruit only the PH domain of PRG (called optoPH), while looking at the basal RhoA activity. In some

cells, we could see a very clear immediate decrease of the biosensor intensity following optoPH recruitment, very similar in terms of dynamics to the decrease observed in highly expressing cells (**Figure 4B-D**). This decrease was significant on the mean but not clearly visible in all cells (**Supp Figure 3**), which was expected since the PH inhibition should depend strongly on the basal RhoA activity that might be mild in resting cells. Our result confirmed that the PH domain of PRG alone can inhibit RhoA activity, probably through a direct binding as proposed in [22] (**Figure 4D**).

Next, we wondered whether such an inhibition plays a role in the protruding phenotype we observe with optoPRG. To test this, we mutated our optoPRG with a double mutation (F1044A and I1046E) known to prevent binding of the PH domain of PRG to RhoA-GTP [22]. This dual mutation had a strong effect on our optogenetic activations, restricting the phenotypes to only the retracting ones, even at high basal concentrations (**Figure 4E,F**). We concluded that the PH domain of optoPRG must bind to RhoA-GTP for the protruding phenotype to happen; either before the activation - to change the cell state - or during recruitment - to prevent RhoA activity. To discriminate between these two hypotheses, we overexpressed the DH-PH domain alone in another fluorescent channel (iRFP) and recruited the mutated PH at the membrane. We still had a large majority of retracting phenotype even in highly expressing cells (**Figure 4G**), showing that the PH binding to RhoA-GTP during recruitment is a key component of the protruding phenotype. Few cells with very high PRG concentration still displayed small ruffles, indicating that even if much less efficient, optoPRG with mutated PH could still trigger protrusions.

These experiments suggest a necessary role of the PH domain of optoPRG for protrusions, but is it sufficient? To check this, we looked at the phenotypic response of cells that overexpress PRG, where we only recruit the PH domain. We could not see either clear protrusion or retraction happening following PH recruitment, as shown by membrane displacement in **Figure 4H,I**. Thus, the inhibitory function of the PH domain is not sufficient for triggering protrusions. This points to the activation of another effector, actively responsible for protrusion formation.

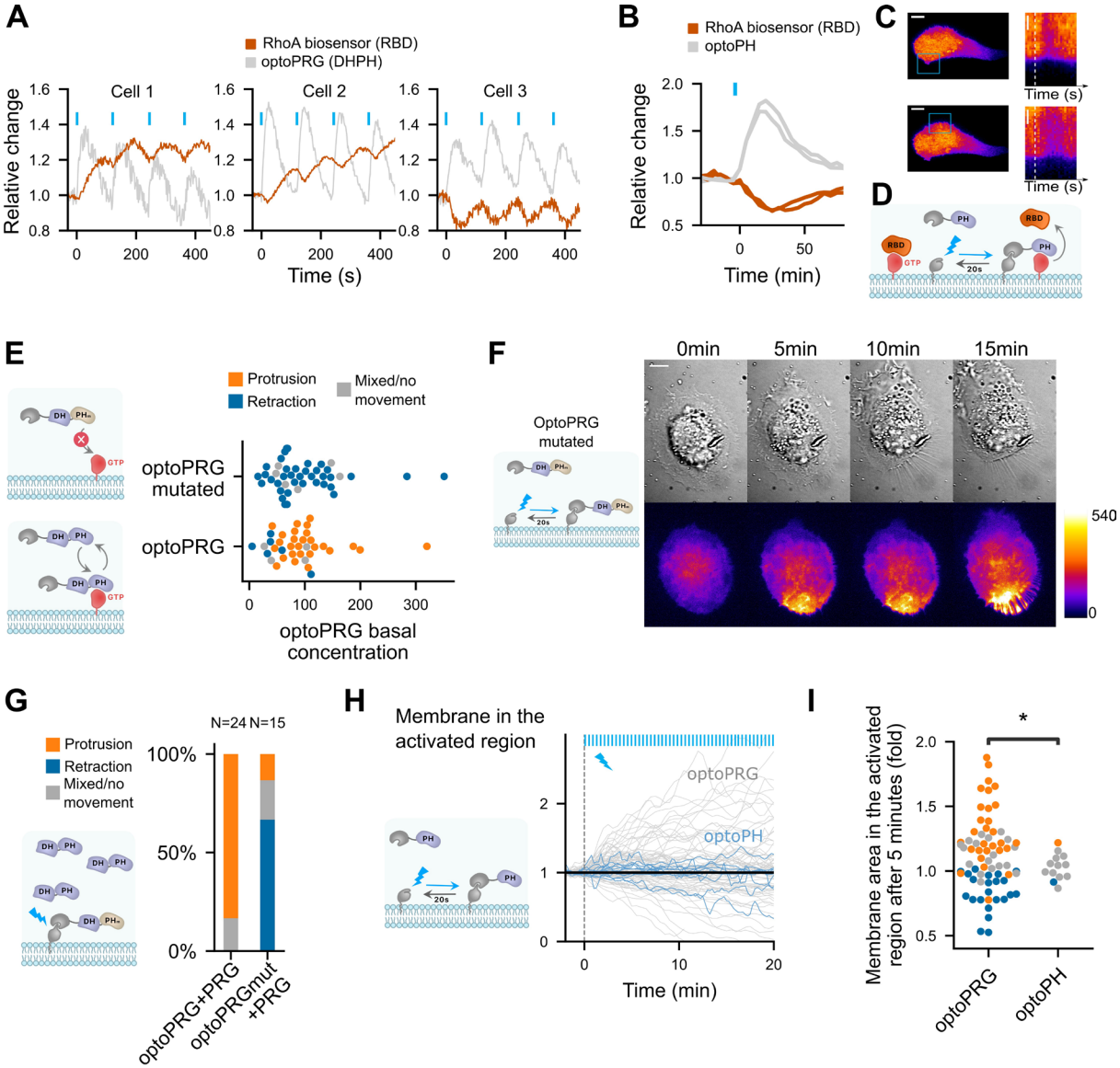

Figure 4: PH domain of PRG is triggering inhibition of RhoA at high PRG concentration and is necessary but not sufficient for protruding phenotype. (**A**) Three representative cells that show very different responses to optoPRG pulsatile activation. Cell 1 has a low optoPRG expression, while Cell 2 and Cell 3 have high concentration of optoPRG. Intensities are normalized by the mean intensity before the first activation (t=0). (**B**) Quantification of the relative change in RhoA biosensor (RBD) after one pulse of optogenetic recruitment of the PH domain of PRG. In gray, optoPH recruitment, in red, RhoA biosensor. Light pulses are shown with blue bars. (**C**) Image of the corresponding cell. On the right, kymograph taken within the activation region. White dotted line shows the starting point of the activation. Scale bar: 10 µm. Region of activation is shown is the blue rectangle. (**D**) Scheme of the probable mechanism of PH domain dominant negative effect on RhoA. **(E)** Phenotype after optogenetic activation for optoPRG (bottom) and optoPRG with the PH mutated for no binding to RhoA-GTP (top). On the left, schemes of the expected behavior of the corresponding proteins. (**F**) Representative image of a cell transfected with the optoPRG with mutated PH, doing a retraction despite the high optoPRG concentration. (**G**) Quantification of protruding and retracting phenotypes in cells highly overexpressing non-recruitable PRG, comparing mutated and non-mutated optoPRG, with a scheme of the experiment on the left. See **Supp Figure 6** for the selected cells. (**H**) Membrane displacement of optoPH cells (in blue) compared to optoPRG cells (in gray). No specific protrusion can be seen. (**I**) Normalized membrane area after 5 minutes in the activated for optoPRG and optoPH cells. Orange: protruding cells, gray: mixed phenotype or no movement, blue: retracting cells.

optoPRG activates Cdc42

To find the active process involved in the protruding phenotype, we turned to the two other best-known GTPases, Rac1 and Cdc42, which are main drivers of cell protrusions. Indeed, a recent work showed that the DH-PH domain of PRG was able to bind Cdc42 and activate it, thanks to conformational change operated by $G\alpha_S$ [26]. To look at the dynamic activity of Rac1 and Cdc42, we first used a Pak Binding Domain (PBD) fused to iRFP. PAK is known for being an effector of both Rac1 and Cdc42, but more sensitive as a biosensor of Cdc42 [27]. After optogenetic activation, we saw an increase in PBD intensity in both the protruding and retracting phenotypes. After one minute, PBD intensity continuously increases for the protruding phenotype while it remains unchanged for the retracting phenotype (**Figure 5A-C**). This suggested an immediate activation of Rac1 or Cdc42 after recruitment of optoPRG, that would be inhibited after few minutes in the case of the retracting phenotype.

We then turned to recently published biosensors that are more specific to Rac1 and Cdc42 [28]. It revealed that Cdc42 is the Rho-GTPase specifically activated immediately after optogenetic activation (**Figure 5D-F**), Rac1 being activated afterwards and only in the protruding phenotype (**Figure 5G-I**), most probably due to the positive feedback between Cdc42 and Rac1 [13]. It also confirmed that Cdc42 was activated in both phenotypes just after the optogenetic recruitment but kept being activated only in the case of the protruding phenotype.

To confirm that Cdc42 activation was necessary for the protrusion, we performed an experiment with IPA3, a drug targeting PAK, one of the direct effectors of Cdc42. We did a first optogenetic activation with a set of cells to know their phenotypes, then incubated our sample five minutes with 5 µM IPA3 and activated the cells again (**Figure 5J**). A lot of cells became round, and none of them were able to protrude again upon optogenetic activation, while retracting ones were often still able to retract (**Figure 5K**). Some previously protruding cells were even able to change phenotype and retract after drug incubation (**Figure 5J,K**). This confirmed us that activation of PAK through Cdc42 was required for the protruding phenotype to happen, but not for the retracting one.

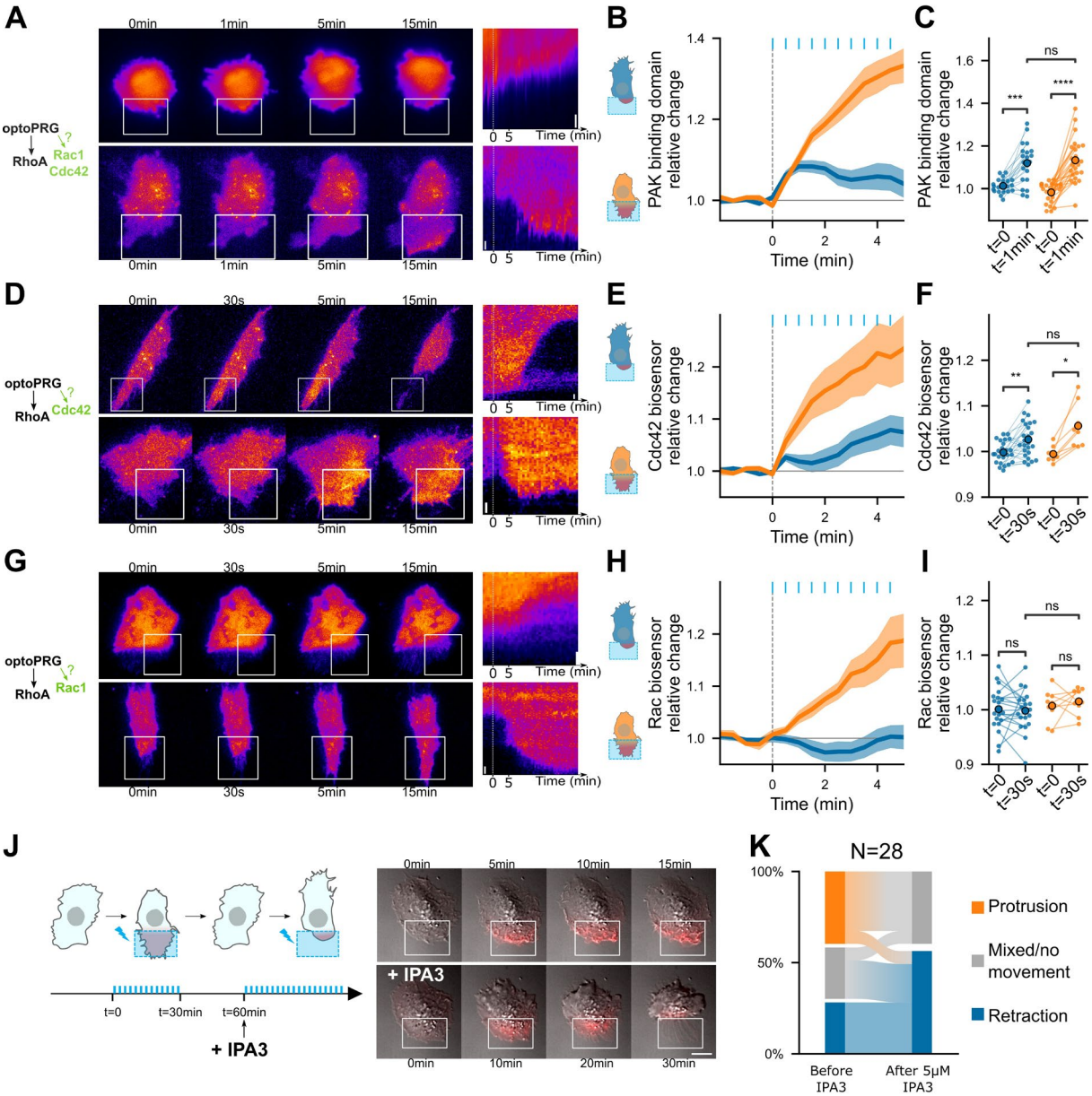

Figure 5: PRG activates Cdc42 and Cdc42 downstream activity is necessary for the protrusive phenotype. (A,D,G) Representative time-lapse images and kymographs of retracting (top) and protruding (bottom) cells labeled with PBD-iRFP (**A**), delCMV-mCherry-WaspGBD (**D**), and mCherry-3xp67Phox (**G**) biosensors [28], activated with optoPRG starting at t=0min. White rectangles are areas of optogenetic activation. Scale bars are 10 µm. (**B,E,H**) Corresponding mean normalized intensities are plotted against time (mean +/- s.e.m.), blue for retracting cells and orange for protruding one. (**C,F,I**) Corresponding pairwise comparison for each cell of the signal inside the region of activation between the initial time and 60s (PBD biosensor) or 30s (Cdc42 and Rac1 biosensors). Data are grouped by phenotype. *P<0.05 **P<0.01, ***P<0.001, **** P<0.0001 (Wilcoxon test to compare t=0 and t>0, independent t-test otherwise). (**J**) Left, scheme describing the IP3 experiment. Blue bars represent optogenetic pulses (every 30s). Half an hour after the first experiment, IPA3 is added at 5 µM. Right, representative cell showing a protruding phenotype with ruffles (top), and a retracting phenotype after addition or IPA3 (bottom). (**K**) Quantification of phenotype switches.

An effective model recapitulates RhoA activity dynamics and enables a control of both phenotypes in the same cell

Given the complexity of all interactions happening and the quantitative nature of our findings, we sought for a minimal model that would capture RhoA biosensor dynamics and the phenotype switch

as a function of optoPRG basal concentration. We also wanted to see if we could play with the quantitative properties of the light stimulation to control both phenotypes in the same cell.

To model RhoA dynamics within a region of the cell, we considered a simple reaction scheme (**Figure 6A**) where inactive RhoA is activated by the GEF (optoPRG) following mass action kinetics. The GEF can be either free or bound to active RhoA thanks to its PH domain. This complex between RhoA-GTP and the GEF, noted *GR*, is inhibiting RhoA downstream activity by titrating active RhoA but does not prevent GEF activity, as shown in [22]. The formation of the complex is characterized by the dissociation constant K_b. Active RhoA is assumed to be deactivated by endogenous GAP at a rate k_2, which sets the characteristic delay between GEF and RhoA-GTP dynamics, putting aside the formation of the complex *GR*. During an optogenetic activation, we assumed that the amount of the GEF, called G_{tot}, is changing because of local concentration increase by membrane recruitment. Introducing the dimensionless variables $r = R/R_{\mathrm{eq}}$ and $g = G_{\mathrm{tot}}/G_{\mathrm{eq}}$, G_{eq} and R_{eq} being the values at equilibrium, and making a quasi-steady state approximation (see **Supp Note** for a detailed derivation of the model) we obtain the following main equation for the relative evolution of actively signaling RhoA:

$$\frac{dr}{dt} = \frac{1}{1 + \frac{G_{\mathrm{eq}}}{K_b} \cdot g} \left(k_2 (g - r) - \frac{G_{\mathrm{eq}}}{K_b} \cdot r \frac{dg}{dt} \right).$$

This equation, which predicts the temporal evolution of active and free RhoA, r, for any given time dependent GEF curve, g, can be solved numerically and depends on only two variables, k_2 and G_{eq}/K_b. The first variable k_2 can be independently estimated from optogenetic experiments with low amounts of optoPRG, for which the formation of the complex is negligible. By first estimating the kinetics of the RBD biosensor that binds RhoA-GTP ($k_{\mathrm{off}} = 0.08 \pm 0.4\ \mathrm{s}^{-1}$), we found that $k_2 = 0.014 \pm 0.003\ \mathrm{s}^{-1}$ (**Supp Note**). We are left with only one free parameter, G_{eq}/K_b , which characterizes the basal level of expression of the optoPRG with respect to the typical concentration at which the complex *GR* forms. This parameter changes from cell to cell, depending on the transfection efficiency. Remarkably, we could reproduce the whole family of RhoA dynamics shown in **Figure 4A** adjusting this single parameter (**Figure 6B**), even if not all experimentally observed curves (**Supp Figure 4**), probably because our model lacks an auto-amplification process. Despite its limitation, we can consider the model describing RhoA response to optoPRG recruitment as a good representation of what is happening at both low and high concentrations of optoPRG.

To model the phenotype, we next added the activation of Cdc42 by the GEF (**Figure 6C**). To keep our model as simple as possible, we assumed that the deactivation rate of Cdc42 was equal to k_2. We hypothesized that the activity of RhoA was in competition with the activity of Cdc42, and that the resulting binary phenotype was the outcome of this competition, which may involve numerous feedbacks and crosstalks. We modeled this competition by a single number γ, which computes the relative difference between integrated activities of RhoA and Cdc42 during the two first minutes after activation – approximately the time at which the phenotype is experimentally seen. As we have access to relative amounts only, we arbitrarily set the relative contribution of RhoA versus Cdc42 such that when γ is positive the cell retracts, and when negative the cell protrudes. We added a gray zone around γ=0 (or equivalently when $G_{\mathrm{eq}}/K_b \sim 0.5$) to take into account the mixed phenotypes. The **Figure 6D** shows the dependence of γ as a function of G_{eq}/K_b: the curve is monotically decreasing; at low G_{eq}/K_b RhoA and Cdc42 dynamics are almost identical but since RhoA dominates Cdc42 the cell

retracts, while at high G_{eq}/K_b RhoA is transiently inhibited by the formation of the complex and Cdc42 can dominate leading to a protrusion.

Having in hands an effective model of the phenotype, we could then explore all possible temporal patterns of activation that correspond to a family of functions $g(t)$. Given the experimental constraints of our optogenetic tool, we focused on the frequency and duration of the light pulses while taking the observed values for *on* and *off* dynamics of the iLID-SspB recruitment. We first looked at the impact of the duration of the pulse, which influences the fold increase of the function g after one pulse of activation. Experimentally, we could go from a fold increase of 1.1 (to be measurable) up to 3. In our model, no cell was able to switch from retracting to protruding or vice versa by only changing the intensity of the optogenetic pulse (**Supp Figure 7**). Then, we looked at the influence of the frequency of the light pulses on the phenotype. Interestingly, for intermediate values of $G_{\mathrm{eq}}/K_b \sim 0.5$ we found that high frequencies lead to protruding phenotypes while low frequencies lead to retracting ones (**Figure 6E**). This result suggests that one could switch the phenotype is a single cell by selecting it for an intermediate expression level of the optoPRG. To verify this theoretical prediction, we screened automatically cells that expressed optoPRG at a level corresponding to the transition from one phenotype to the other (14-35 a.u., see **Figure 2A**). While the majority of cells showed mixed phenotypes irrespectively of the activation pattern, in few cells (3 out of 90) we were able to alternate the phenotype between retraction and protrusion several times at different places of the cell by changing the frequency while keeping the same total integrated intensity (**Figure 6F** and **Supp Movie X**).

Our model can be summarized by the following picture (**Figure 6G**). At low concentration of the GEF, both RhoA and Cdc42 are activated by optogenetic recruitment of optoPRG, but RhoA takes over. At high GEF concentration, recruitment of optoPRG lead to both activation of Cdc42 and inhibition of already present activated RhoA, which pushes the balance towards Cdc42. In the end (**Figure 6H**), optogenetic modulation of PRG can be seen as moving the balance between RhoA and Cdc42 depending on the basal state. This means that only the cells in good concentration range can use the same protein to control both antagonist responses.

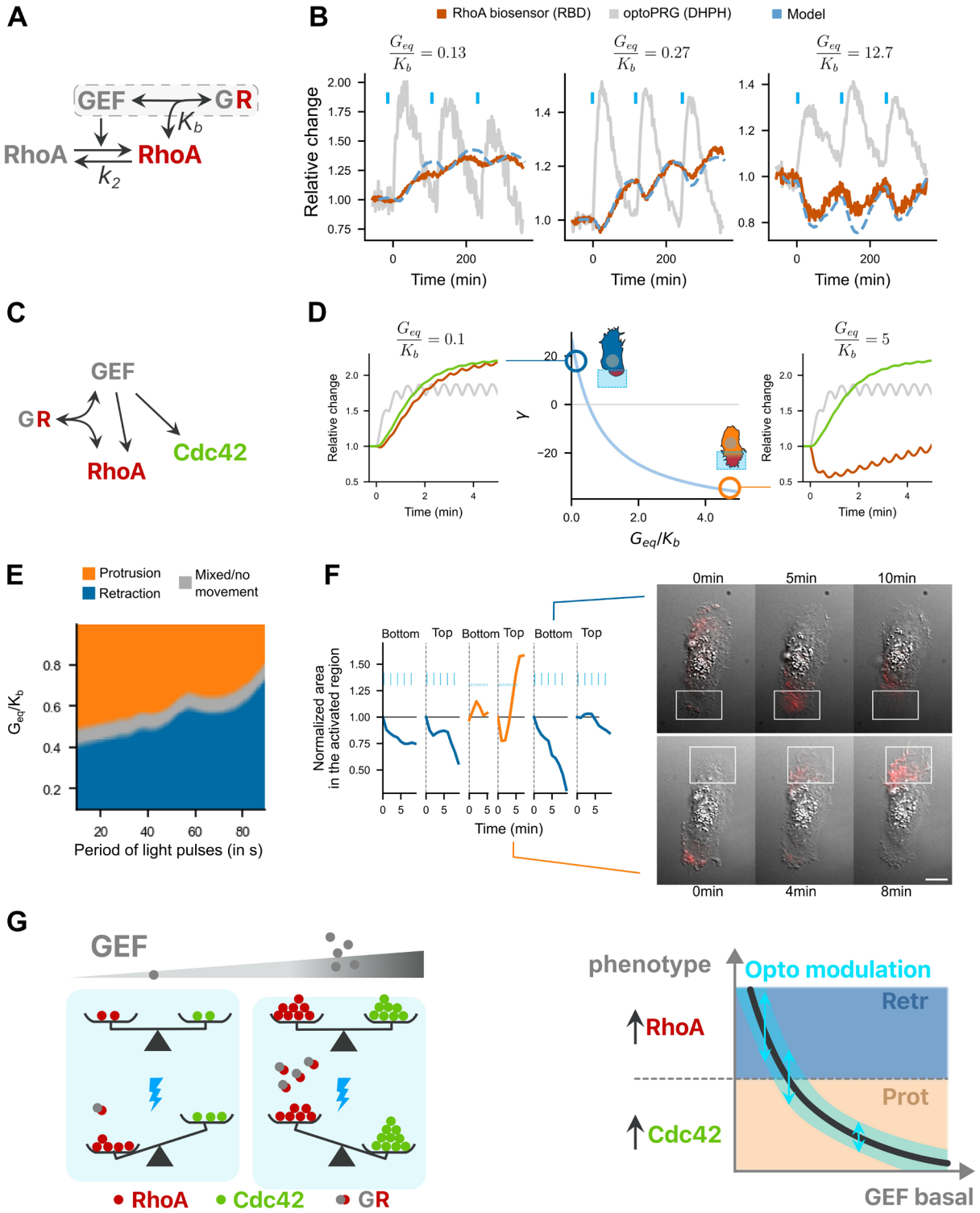

Figure 6: a minimal model recapitulates RhoA activity dynamics and the phenotypic switch. (**A**) Model for active RhoA dynamics. Interactions are represented with arrows, with the two main parameters of the model. (**B**) The three different RhoA dynamics are well fitted with one single free parameter, G_{eq}/K_b. Dotted blue line: fitted curve, with gray line $g(t)$ taken as input (optoPRG recruitment). Red line: RBD biosensor. (**C**) Complete model, adding Cdc42 to (A): the GEF PRG can activate both RhoA and Cdc42, but can also inhibit RhoA by directly binding to it. (**D**) Center, evolution of γ describing the phenotype (positive for retraction and negative for protrusion) against the free parameter G_{eq}/K_b. Two representative dynamics are shown on the right and on the left for the same input $g(t)$, for a low and high G_{eq}/K_b. In grey, optoPRG recruitment to the membrane, in green, Cdc42

activity, in red, RhoA activity. (**E**) Map of the phenotype as function of the free parameter G_{eq}/K_b and of the duration time between two pulses. (**F**) One example of two phenotypes controlled in the same cell. On the left, first ten minutes of the cell area in the illuminated region for different frequencies and intensities of activation (low frequency high power every 30s, high frequency low power every 15s). On the right, two representative timelapse of retraction (top) and protrusion (bottom), activation is shown with the white rectangle. Scale bar: 10µm. (**G,H**) Graphical conclusion on the model. (G) Balance between RhoA and Cdc42 activity is represented in function of GEF basal concentration (grey gradient), both at the basal state (top) and after optogenetic activation (bottom, with blue lightning). At low concentrations RhoA takes over. At high concentration, optoPRG binds to active RhoA and inhibits it (complex *GR*), which enables Cdc42 to take over. (H) Curve showing the difference between RhoA and Cdc42 activity as a function of the basal intensity of the GEF. Phenotypes are marked with the colors (blue, retraction and orange, protrusion). Optogenetic modulation happens on vertical line, with the blue range, which limits the possibility of switching from one phenotype to the other.

Discussion

Using the DH-PH domain of PRG, we have shown that its local recruitment to the plasma membrane can result in two opposite phenotypes: a protrusion in the activation region when highly expressed, or a retraction in the same region when expressed at low concentrations. The known ability of the DH-PH domain to activate RhoA was confirmed in the case of retraction phenotypes. However, in protruding phenotypes, it negatively regulated RhoA activity in the first minutes after optogenetic perturbations and simultaneously activated Cdc42. These findings were summarized in a simple model that recapitulated the various experimental results. It predicted that cells with intermediate concentrations of the optogenetic actuator could show both phenotypes depending on the frequency of the light pulses. We verified experimentally that it was the case, confirming that we had captured the main features of the underlying biochemical network.

The ability of PRG to induce the two phenotypes is supported by previously reported direct interactions. First and most obviously, the activation of RhoA by the he DH-PH domain of PRG has been well documented, the structure of the complex is even known [29]. The ability of PRG DH-PH to greatly enhance RhoA-GDP switch to RhoA-GTP has been studied *in vitro* with purified proteins [30]. This enhancement is assumed to come from the positive feedback loop by which RhoA in its active GTP form recruits the GEF through its interaction with the PH domain [22], leading to more activation of RhoA. However, this feedback loop can turn into a negative one for high level of GEF: the direct interaction between the PH domain and RhoA-GTP prevents RhoA-GTP binding to effectors through a competition for the same binding site. Along this line, it was shown that overexpressing the PH domain alone reduced RhoA activity [22]. Second, the direct interaction of the DH-PH domain of PRG with Cdc42-GDP and its ability to enhance the switch to Cdc42-GTP has been shown in a previous work [26]. Notably, the linker region between the DH and the PH domain is required for effective interaction, as well as $\mathrm{G}_{\alpha s}$ activity.

Our observation of the double phenotype appeared to be a relatively general feature since we obtained it in another cell line and with at least one other GEF of RhoA. However, the protruding phenotype happened rarely with the DH-PH domain of GEF-H1, and we could not observe it at all with the DH-PH of LARG, another GEF of RhoA from the Dbl family. Thus, the precise biochemical natures of GEF domains are of importance. The interactions of the PH domain of GEF-H1 and LARG with RhoA-GTP have been described in [31]: GEF-H1 PH domain has almost the same inhibition ability than PRG PH domain, while LARG PH domain is less efficient. Moreover, it seems that LARG DH-PH domain has no

effect on Cdc42 [26], while nothing is known for GEF-H1 DH-PH domain. As a consequence, the fact that PRG DH-PH is able to trigger protrusions reproducibly compared to other GEFs could be explained by its ability to efficiently inhibit RhoA-GTP while activating Cdc42 at the same time. These two combined properties would allow the GEF to be expressed at a high basal level required for the protruding phenotype since the inhibition by the PH domain prevents RhoA overactivation and Cdc42 activation prevents cell rounding through its competition with RhoA. This could also explain the increase in cell size for protruding cells. Supporting this hypothesis, we observed that expressing transiently optoGEF-H1 and optoLARG was much harder than for optoPRG, many cells becoming round or dying when positively transfected.

Interestingly, PRG is known for its role in cell migration, both at the rear [32] and at the front [28]. Given that FRET measurements that are sensing GEFs activity report RhoA activity at the protruding front [11] and biosensors of RhoA-GTP report activity at the retracting back [25], our results might solve this paradox: PRG would activate Cdc42 at the front meanwhile activating RhoA at the back. PRG is also known for being prometastatic and is overexpressed in different cancers favoring migration and epithelial to mesenchymal transition [33–35]. In these pathological cases, PRG was studied as a promoter of RhoA activity. However, our results point clearly towards a possible switch in PRG role when overexpressed, acting more on Cdc42 activity. Such a switch in function could be a mechanism happening for other GEFs or proteins and should be considered when designing therapies.

We demonstrated that changing the dynamics of one single protein is enough to switch its function when being recruited to the membrane. Even if the context was quite specific (cells with a specific concentration), such multiplexing may be happening in vivo, where dynamics and local concentrations can highly vary in the cytoplasm and in different subcellular domains. We were limited here by the dynamic of the optogenetic dimer, but endogenous interactions may be more refined, and therefore used by the cell to multiplex signals. The fact that a protein can have different functions based on its dynamics is not new [1]. However, examples that demonstrate a causal relationship between activation of a protein and opposite cellular responses exist mostly at the transcriptional level, on the timescale of hours [2]. To our knowledge, there are only two examples, both involving optogenetics, of such a dual response on shorter time scales and for protein-protein interactions. In the first example, it was shown that two different acto-adhesive structures could form in response to either Src recruitment or clustering [36]; the specificity being encoded here by the dynamics of Src nanoclusters at the adhesive sites. In the second example, RhoA activation by uncaging of a GEF of RhoA triggered focal adhesion growth via Src activation only at submaximal levels, revealing a selection of cellular response by signal amplitude [23].

Altogether, we have revealed and explained a striking example of protein multiplexing, while underscoring the crucial role of protein dynamics for signal transduction. We have also raised open questions about the link between signaling proteins and their functions, particularly in contexts where they are highly overexpressed, as often observed in cancer.

Acknowledgements
We thank Leo Valon for scientific discussions and initial development of the optogenetic activation of RhoA. We thank Guilhem Glaziou for some preliminary experiments. The work was done with support from the LabEx Cell(n)Scale (ANR-10-LABX-0038), Labex and Equipex IPGG (ANR-10-NANO0207), Idex

Paris Science et Lettres (ANR-10-IDEX-0001-02 PSL), French National Research Infrastructure France-BioImaging (ANR-10-INBS-04), Institut Convergences Q-life (ANR-17-CONV-0005). JDS thanks AMX from Ecole Polytechnique and the ARC foundation.

Declaration of Interests

The authors declare no competing interests.

Material and methods

Cell culture. hTERT RPE1 cells (CRL-4000 strain, ATCC, Manassas, VA) were cultured at 37°C with 5% CO2 in Dulbecco's modified Eagle's/F-12 medium supplemented with 10% fetal bovine serum, GlutaMAX (2 mM) and penicillin (100 U/mL)-streptomycin (0.1 mg/mL). Cells were passaged twice a week in a ratio of 1/10 by washing them with PBS (1X) solution and dissociating using TrypLE Express (Thermo Fisher Scientific, Waltham, MA) reagent for 3 to 5 minutes.

Plasmids: dTomato-2xrGBD (Plasmid #129625) (RhoA biosensor), pLL7:Venus-iLID-CAAX (#60411), 2XPDZ-mCherry-Larg(DH) (Plasmid #80407) plasmids were bought from Addgene (Watertown, MA). pLVX: MRLC-iRFP, pLVX: Lifeact-iRFP pLVX: PBD-iRFP (PAK biosensor) plasmids were made by Simon de Beco (Institut Curie, France). pCMV:PRG(DHPH)-RFPt-SspB-P2A-mVenus-iLID-CAAX is a gift from Alessandra Casano (EMBL). pLL7:PRG(DHPH)-iRFP-SspB-P2A-mVenus-iLID-CAAX was subcloned by Maud Bongaerts (Institut Curie, France) from PRG(DHPH)-CRY2-mCherry and pLL7:VenusiLID-CAAX. pCMV:PRG(PH)-iRFP-SspB-P2A-mVenus-iLID-CAAX was subcloned by Benoit Boulevard (Institut Curie, France) from pCMV:PRG(DHPH)-RFPt-SspB-P2A-mVenusiLID-CAAX. pCMV:PRG(PH)-RFPt-SspB-P2A-mVenus-iLID-CAAX was designed in the lab and synthesized by Twist Bioscience (Twist Bioscience, San Francisco). Rac1 and Cdc42 biosensors, delCMV-mCherry-3xp67Phox and delCMV-mCherry-WaspGBD respectively, described in [Nanda et al., 2023], were gifts from Leif Dehmelt (Dortmund and Max Planck Institute of Molecular Physiology).

Transfection: Transfections were performed using jetPRIME®versatile DNA/siRNA transfection reagent according to the manufacturer's protocol. Different ratio of plasmid DNA were used depending on the constructs, and a ratio of 2:1 of transfection reagent and DNA. Experiments were performed at least 30 hours after DNA transfection, and 48 hours after siRNA transfection.

Drug assay : For IPA-3 (p21-Activated Kinas Inhibitor III, CAS 42521-82-4, Calbiochem), between 20 to 30 cells were first selected and optogenetically activated for 30 minutes. 30 minutes after the end of the first activation, the medium was replaced by the drug diluted in complete DMEM/F-12 medium at specified concentrations, and optogenetic activation was done again five minutes after medium replacement.

Imaging: Imaging was performed at 37 °C in 5% CO2. Two different microscopes have been used: an IX83 and an IX71 (Olympus, Melville, NY) both with inverted fluorescence and Differential Interference Contrast (DIC) and controlled with MetaMorph software (Molecular Devices, Eugene, OR). Both microscopes were equipped with a 60x objective (NA=1.45), motorized stage and filter wheel with SmartShutter Lambda 10-3 control system (Sutter Instrument Company, Novato, CA), a stage-top

incubation chamber with temperature and CO2 control (Pecon, Meyer Instruments, Houston, TX), a laser control system with azimuthal TIRF configuration (iLas2, Roper Scientific,Tucson, AZ). The IX71 was equipped with an ORCA-Flash5.0 V3 Digital CMOS camera (Hamamatsu Photonics K.K., Japan), a z-axis guiding piezo motor (PI, Karlsruhe, Germany) a CRISP autofocus system (ASI, Eugene, OR), and a DMD pattern projection device (DLP Light Crafter, Texas instruments, Dalas, TX), illuminated with a SPECTRA Light Engine (Lumencor, Beaverton, OR) at 440±10 nm. The IX83 has a built in z-piezo and autofocus, and was equipped with a Evolve EMCCD camera (Photometrics, Tucson, AZ) and a FRAP configuration (iLas2, Roper Scientific, Tucson, AZ).

Local optogenetic illumination : Local illumination was performed thanks to a DMD placed on the optical path. DMD used in the experiments was a DLP4500 with a LC4500 controller from Keynote Photonics (Keynotes Photonics, Allen, TX). The chip has a dimension of 1140 x 912 micromirrors (6161.4µm x 9855µm), able to generate 8-bit grayscale patterns. We generated custom illumination patterns using the DMD and a blue LED illumination source (SPECTRA Light Engine (Lumencor, Beaverton, OR).

Cell finder: To find transfected cells on coverslips with a wide range of fluorescence intensities, working with single cells, we developed a small Python software (Python Software Foundation. Python Language Reference, version 3.9.5.), which we named **Cell finder**, that greatly facilitates the search for transfected cells. This software, available on Github https://github.com/jdeseze/cellfinder), scans the entire available area, finds any fluorescent object larger than a predefined size (with a threshold to define what is fluorescent), and produces the resulting list of locations in customized format for the Metamorph imaging software. If the number of cells found is too important, I create a Python-based GUI interface to select only the desired positions based on the image acquired during the search trajectory. It allows seeding cells at low density to scatter them, and still have dozens of transfecting cells within one 25mm-coverslip for the experiments.

Image analysis: All image analyses have been done with homemade script, using Python (Python Software Foundation. Python Language Reference, version 3.9.5.) through the napari interface [Chiu and Clack, 2022]. All movies are created with Fiji, as well as picture montages. The kymographs have been done thanks to the *Reslice* function in Fiji, with different linewidths depending on the with of the cell. Quantification have been done thanks to custom plugins for napari imaging software [Chiu and Clack, 2022] developed in the lab and available on github (https://github.com/jdeseze/napari-intensitymeasurements). Segmentation used optical flow Farneback algorithm in a similar way than in [Robitaille et al., 2022] for membrane displacement measurement, or classical thresholding of fluorescent channel for intensity measurements.

Data processing *Surface displacement* : Surface displacement is the area of the intersection between the activated area and cell segmentation. *Normalization* : Biosensors intensities are calculated the following way. First, background is subtracted. Second, mean intensity in the intersection between activated area and cell segmentation is calculated. Third, this intensity is divided by the mean intensity in the non-activated part of the cell. Fourth the intensity is normalized by the intensity before the optogenetic activation. *Dotplots of intensities* : the normalized curved at the specific timepoints specified in each figures are plotted as swarmplots, with the means. *Images and movies* : for DIC images, raw image is divided by the gaussian-filtered image with a large diameter, from 30 to 50 pixels,

to correct for uneven illumination. *Sankey diagrams* : sankey diagrams were done by modifying a python library called pySankey (https://pypi.org/project/pySankey/). *Persistence* : persistence was calculated as the ratio between the actual distance from the initial point and the sum of the absolute value of all displacements. *Myosin ratio* : clusters were cut it in half along the x-axis, and the ratio between left (activated) and right (non-activated) part was measured.

Modelling : The modelling was performed with Python software (Python Software Foundation. Python Language Reference, version 3.9.5.). The differential equations were integrated thanks to the *odeint* function from scipy.integrate package, and all the fitted parameters were found by the least squares method, using *fmin_powell* function from scipy.optimize for minimization, which uses Powell minimization's method.

References

1. Purvis, J.E., and Lahav, G. (2013). Encoding and Decoding Cellular Information through Signaling Dynamics. Cell *152*, 945–956. 10.1016/J.CELL.2013.02.005.

2. Toettcher, J.E., Weiner, O.D., and Lim, W.A. (2013). Using optogenetics to interrogate the dynamic control of signal transmission by the Ras/Erk module. Cell *155*, 1422–1434. 10.1016/j.cell.2013.11.004.

3. Ridley, A.J., Schwartz, M.A., Burridge, K., Firtel, R.A., Ginsberg, M.H., Borisy, G., Parsons, J.T., and Horwitz, A.R. (2003). Cell Migration: Integrating Signals from Front to Back. Science (1979) *302*, 1704–1709. 10.1126/science.1092053.

4. Lahav, G., Rosenfeld, N., Sigal, A., Geva-Zatorsky, N., Levine, A.J., Elowitz, M.B., and Alon, U. (2004). Dynamics of the p53-Mdm2 feedback loop in individual cells. Nat Genet *36*, 147–150. 10.1038/NG1293.

5. Jaffe, A.B., and Hall, A. (2005). Rho GTPases: Biochemistry and biology. Annu Rev Cell Dev Biol *21*, 247–269. 10.1146/ANNUREV.CELLBIO.21.020604.150721.

6. Dolmetsch, R.E., Lewis, R.S., Goodnow, C.C., and Healy, J.I. (1997). Differential activation of transcription factors induced by Ca2+ response amplitude and duration. Nature *386*, 855–858. 10.1038/386855A0.

7. Cherfils, J., and Zeghouf, M. (2013). Regulation of small GTPases by GEFs, GAPs, and GDIs. Physiol Rev *93*, 269–309. 10.1152/PHYSREV.00003.2012/SUPPL_FILE/TABLES1.PDF.

8. Hall, a (1998). Rho GTPases and the actin cytoskeleton. Science *279*, 509–514.

9. Pertz, O. (2010). Spatio-temporal Rho GTPase signaling - where are we now? J Cell Sci *123*, 1841–1850. 10.1242/jcs.064345.

10. Machacek, M., Hodgson, L., Welch, C., Elliott, H., Pertz, O., Nalbant, P., Abell, A., Johnson, G.L., Hahn, K.M., and Danuser, G. (2009). Coordination of Rho GTPase activities during cell protrusion. Nature *461*, 99–103. 10.1038/nature08242.

11. Pertz, O., Hodgson, L., Klemke, R.L., and Hahn, K.M. (2006). Spatiotemporal dynamics of RhoA activity in migrating cells. Nature *440*, 1069–1072. 10.1038/NATURE04665.

12. Worthylake, R.A., Lemoine, S., Watson, J.M., and Burridge, K. (2001). RhoA is required for monocyte tail retraction during transendothelial migration. J Cell Biol *154*, 147. 10.1083/JCB.200103048.

13. de Beco, S., Vaidziulyte, K., Manzi, J., Dalier, F., di Federico, F., Cornilleau, G., Dahan, M., and Coppey, M. (2018). Optogenetic dissection of Rac1 and Cdc42 gradient shaping. Nat Commun *9*, 4816. 10.1038/s41467-018-07286-8.

14. Vaidžiulytė, K., Macé, A.S., Battistella, A., Beng, W., Schauer, K., and Coppey, M. (2022). Persistent cell migration emerges from a coupling between protrusion dynamics and polarized trafficking. Elife *11*. 10.7554/ELIFE.69229.

15. Chandrasekar, S., Beach, J.R., and Oakes, P.W. (2023). Shining a light on RhoA: Optical control of cell contractility. Int J Biochem Cell Biol *161*, 106442. 10.1016/J.BIOCEL.2023.106442.

16. de Seze, J., Gatin, J., and Coppey, M. (2023). RhoA regulation in space and time. FEBS Lett *597*, 836–849. 10.1002/1873-3468.14578.

17. Guntas, G., Hallett, R.A., Zimmerman, S.P., Williams, T., Yumerefendi, H., Bear, J.E., and Kuhlman, B. (2015). Engineering an improved light-induced dimer (iLID) for controlling the localization and activity of signaling proteins. Proceedings of the National Academy of Sciences *112*, 112–117. 10.1073/pnas.1417910112.

18. Inaba, H., Miao, Q., and Nakata, T. (2021). Optogenetic control of small GTPases reveals RhoA mediates intracellular calcium signaling. Journal of Biological Chemistry *296*. 10.1016/j.jbc.2021.100290.

19. O'Neill, P.R., Castillo-Badillo, J.A., Meshik, X., Kalyanaraman, V., Melgarejo, K., and Gautam, N. (2018). Membrane Flow Drives an Adhesion-Independent Amoeboid Cell Migration Mode. Dev Cell *46*, 9-22.e4. 10.1016/j.devcel.2018.05.029.

20. Kamps, D., Koch, J., Juma, V.O., Campillo-Funollet, E., Graessl, M., Banerjee, S., Mazel, T., Chen, X., Wu, Y.W., Portet, S., et al. (2020). Optogenetic Tuning Reveals Rho Amplification-Dependent Dynamics of a Cell Contraction Signal Network. Cell Rep *33*. 10.1016/J.CELREP.2020.108467.

21. Valon, L., Marín-Llauradó, A., Wyatt, T., Charras, G., and Trepat, X. (2017). Optogenetic control of cellular forces and mechanotransduction. Nat Commun. 10.1038/ncomms14396.

22. Chen, Z., Medina, F., Liu, M.Y., Thomas, C., Sprang, S.R., and Sternweis, P.C. (2010). Activated RhoA binds to the Pleckstrin Homology (PH) domain of PDZ-RhoGEF, a potential site for autoregulation. Journal of Biological Chemistry *285*, 21070–21081. 10.1074/JBC.M110.122549/ATTACHMENT/EC2A2BE2-3501-4060-81B7-070F3C1ED161/MMC1.PDF.

23. Ju, J., Lee, H.N., Ning, L., Ryu, H., Zhou, X.X., Chun, H., Lee, Y.W., Lee-Richerson, A.I., Jeong, C., Lin, M.Z., et al. (2022). Optical regulation of endogenous RhoA reveals selection of cellular responses by signal amplitude. Cell Rep *40*, 111080. 10.1016/J.CELREP.2022.111080.

24. Martin, K., Reimann, A., Fritz, R.D., Ryu, H., Jeon, N.L., and Pertz, O. (2016). Spatio-temporal co-ordination of RhoA, Rac1 and Cdc42 activation during prototypical edge protrusion and retraction dynamics. Scientific Reports 2016 6:1 *6*, 1–14. 10.1038/srep21901.

25. Mahlandt, E.K., Arts, J.J.G., van der Meer, W.J., van der Linden, F.H., Tol, S., van Buul, J.D., Gadella, T.W.J., and Goedhart, J. (2021). Visualizing endogenous Rho activity with an improved localization-based, genetically encoded biosensor. J Cell Sci *134*. 10.1242/JCS.258823.

26. Castillo-Kauil, A., García-Jiménez, I., Cervantes-Villagrana, R.D., Adame-García, S.R., Beltrán-Navarro, Y.M., Gutkind, J.S., Reyes-Cruz, G., and Vázquez-Prado, J. (2020). Gαsdirectly drives PDZ-RhoGEF signaling to Cdc42. Journal of Biological Chemistry *295*, 16920–16928. 10.1074/JBC.AC120.015204/ATTACHMENT/F8658DD4-1367-4B5B-920F-899371685E0C/MMC2.PDF.

27. Mahlandt, E.K., Palacios Martínez, S., Arts, J.J., Tol, S., van Buul, J.D., and Goedhart, J. (2023). Opto-RhoGEFs, an optimized optogenetic toolbox to reversibly control Rho GTPase activity on a global to subcellular scale, enabling precise control over vascular endothelial barrier strength. Elife *12*. 10.7554/ELIFE.84364.

28. Nanda, S., Calderon, A., Duong, T.-T., Koch, J., Sachan, A., Xin, X., Solouk, D., Wu, Y.-W., Nalbant, P., and Dehmelt, L. (2023). Crosstalk between Rac and Rho GTPase activity mediated by Arhgef11 and Arhgef12 coordinates cell protrusion-retraction cycles. bioRxiv, 2023.02.20.529203. 10.1101/2023.02.20.529203.

29. Derewenda, U., Oleksy, A., Stevenson, A.S., Korczynska, J., Dauter, Z., Somlyo, A.P., Otlewski, J., Somlyo, A. V., and Derewenda, Z.S. (2004). The Crystal Structure of RhoA in Complex with the DH/PH Fragment of PDZRhoGEF, an Activator of the Ca2+ Sensitization Pathway in Smooth Muscle. Structure *12*, 1955–1965. 10.1016/J.STR.2004.09.003.

30. Gasmi-Seabrook, G.M.C., Marshall, C.B., Cheung, M., Kim, B., Wang, F., Jang, Y.J., Mak, T.W., Stambolic, V., and Ikura, M. (2010). Real-time NMR Study of Guanine Nucleotide Exchange and Activation of RhoA by PDZ-RhoGEF. Journal of Biological Chemistry *285*, 5137–5145. 10.1074/JBC.M109.064691.

31. Medina, F., Carter, A.M., Dada, O., Gutowski, S., Hadas, J., Chen, Z., and Sternweis, P.C. (2013). Activated RhoA Is a Positive Feedback Regulator of the Lbc Family of Rho Guanine Nucleotide Exchange Factor Proteins *. Journal of Biological Chemistry *288*, 11325–11333. 10.1074/JBC.M113.450056.

32. Iwanicki, M.P., Vomastek, T., Tilghman, R.W., Martin, K.H., Banerjee, J., Wedegaertner, P.B., and Parsons, J.T. (2008). FAK, PDZ-RhoGEF and ROCKII cooperate to regulate adhesion movement and trailing-edge retraction in fibroblasts. J Cell Sci *121*, 895–905. 10.1242/JCS.020941.

33. Struckhoff, A.P., Rana, M.K., Kher, S.S., Burow, M.E., Hagan, J.L., Del Valle, L., and Worthylake, R.A. (2013). PDZ-RhoGEF is essential for CXCR4-driven breast tumor cell motility through spatial regulation of RhoA. J Cell Sci *126*, 4514–4526. 10.1242/JCS.132381.

34. Du, J., Zhu, Z., Xu, L., Chen, X., Li, X., Lan, T., Li, W., Yuan, K., and Zeng, Y. (2020). ARHGEF11 promotes proliferation and epithelial-mesenchymal transition of hepatocellular carcinoma through activation of β-catenin pathway. Aging *12*, 20235–20250. 10.18632/AGING.103772.

35. Ding, Z., Dhruv, H., Kwiatkowska-Piwowarczyk, A., Ruggieri, R., Kloss, J., Symons, M., Pirrotte, P., Eschbacher, J.M., Tran, N.L., and Loftus, J.C. (2018). PDZ-RhoGEF Is a Signaling Effector for

TROY-Induced Glioblastoma Cell Invasion and Survival. Neoplasia *20*, 1045. 10.1016/J.NEO.2018.08.008.

36. Kerjouan, A., Boyault, C., Oddou, C., Hiriart-Bryant, E., Grichine, A., Kraut, A., Pezet, M., Balland, M., Faurobert, E., Bonnet, I., et al. (2021). Control of SRC molecular dynamics encodes distinct cytoskeletal responses by specifying signaling pathway usage. J Cell Sci *134*. 10.1242/JCS.254599.